Published in final edited form as:
J Control Release. 2014 October 10; 191: 115–122. doi:10.1016/j.jconrel.2014.05.006.

Prolonged Blood Circulation and Enhanced Tumor Accumulation of Folate-Targeted Dendrimer-Polymer Hybrid Nanoparticles

Suhair Sunoqrot[1], **Jason Bugno**[1], **Daniel Lantvit**[2], **Joanna E. Burdette**[1,2], and **Seungpyo Hong**[1,3,*]

[1]Department of Biopharmaceutical Sciences, University of Illinois, Chicago, IL 60612

[2]Department of Medicinal Chemistry and Pharmacognosy, University of Illinois, Chicago, IL 60612

[3]Department of Biongineering, University of Illinois, Chicago, IL 60612

Abstract

Nanoparticle (NP)-based drug delivery platforms have received a great deal of attention over the past two decades for their potential in targeted cancer therapies. Despite the promises, passive targeting approaches utilizing relatively larger NPs (typically 50–200 nm in diameter) allow for passive tumor accumulation, but hinder efficient intratumoral penetration. Conversely, smaller, actively targeted NPs (<20 nm in diameter) penetrate well into the tumor mass, but are limited by their rapid systemic elimination. To overcome these limitations, we have designed a multi-scale hybrid NP platform that loads smaller poly(amidoamine) (PAMAM) dendrimers (~5 nm in diameter) into larger poly(ethylene glycol)-b-poly(*D,L*-lactide) (PEG-PLA) NPs (~70 nm). A biodistribution study in healthy mice revealed that the hybrid NPs circulated longer than free dendrimers and were mostly cleared by macrophages in the liver and spleen, similar to the *in vivo* behavior of PEG-PLA NPs. When injected intravenously into the BALB/c athymic nude mice bearing folate receptor (FR)-overexpressing KB xenograft, the targeted hybrid NPs encapsulating folate (FA)-targeted dendrimers achieved longer plasma circulation than free dendrimers and higher tumor concentrations than both free dendrimers and the empty PEG-PLA NPs. These results suggest that the hybrid NPs successfully combine the *in vivo* advantages of dendrimers and polymeric NPs, demonstrating their potential as a new, modular platform for drug delivery.

*All correspondence should be addressed to: Prof. Seungpyo Hong, Ph.D., Department of Biopharmaceutical Sciences, College of Pharmacy, The University of Illinois at Chicago, 833 S. Wood St. Rm 335, Chicago, IL 60612, Phone: 312-413-8294, Fax: 312-996-0098, sphong@uic.edu.

Supporting information. ^{1}H NMR and UV/Vis spectra, and additional CLSM images of MCTS treated with nontargeted dendrimer conjugates.

1. INTRODUCTION

Over the past two decades, nanotechnology-based drug delivery platforms have shown great promise in reducing the toxic side effects of currently available therapeutic drugs. [1] The controlled size (50–200 nm in diameter) of nanoparticles (NPs) such as liposomes, biodegradable polymeric NPs, and micelles allows their passive accumulation at tumor tissues through the enhanced permeability and retention (EPR) effect. [2–6] However, the therapeutic benefit of the majority of nanocarriers in this size range is limited by inadequate tumor delivery. [7] This is partially attributed to the dense tumor interstitial matrix, which hinders the diffusion of NPs larger than 60 nm, causing them to accumulate in perivascular regions and exert only local effects. [8–11] Conversely, smaller NPs (<20 nm), which can achieve better interstitial transport and tumor penetration, [12–19] are often associated with a shorter blood half-life and fast clearance through renal filtration. In particular, folate (FA)-targeted poly(amidoamine) (PAMAM) dendrimers have previously shown high targeting efficacy to FA receptor (FR)-overexpressing tumor xenografts. [20–25] Unfortunately, their small size (~5 nm in diameter) and the surface exposure of the targeting ligands have been the cause of their short circulation time and significant liver uptake. [24, 26]

To maximize the targeting efficacy of the existing nanocarriers, there is an emerging need to develop a multi-scale system that combines actively targeted smaller NPs possessing favorable tissue penetration and diffusivity, with larger NPs capable of passive targeting and longer blood circulation times. Previously, we have designed a multi-scale hybrid NP platform where FA-targeted generation 4 (G4) PAMAM dendrimers are loaded within larger poly(ethylene glycol)-b-poly(*D,L*-lactide) (PEG-PLA) polymeric NPs (Figure 1).[27–29] The hybrid NPs, or hybrid NPs (~100 nm in diameter), combined the highly selective cellular interactions of FA-targeted dendrimers with the larger size and controlled release properties of polymeric NPs, which dictated their cellular interaction kinetics and uptake pathways by FA receptor (FR)-overexpressing KB cells (KB FR^+) (Figure 2). Simulated penetration assays in multicellular tumor spheroids (MCTS) also revealed that the targeted dendrimers can penetrate deep into the spheroids upon their release from the hybrid NPs, imparting favorable penetration properties as opposed to the polymeric NPs alone. [28]

These preliminary findings highlight the potential of the hybrid NP system to address the limitations faced by FA-targeted dendrimers and polymeric NPs *in vivo.* As illustrated in Figure 1, we hypothesized that by controlling the release of the dendrimer conjugates, the hybrid NP platform could prolong the circulation time of free dendrimers and protect against premature systemic elimination. At the same time, the controlled size of the hybrid NPs may allow them to passively target tumors through the EPR effect. As the hybrid NPs accumulate at the tumor site, actively targeted dendrimers are expected to be gradually released from the biodegradable PEG-PLA matrix, enabling selective targeting to individual cancer cells, with more efficient tumor distribution and penetration (Figure 1).

The targeting efficacy of FA-targeted G5 PAMAM dendrimers has been extensively evaluated *in vitro* and *in vivo*. [22–24] In our previous studies, we employed FA-targeted G4 PAMAM dendrimers, possessing a smaller size (MW 14 kDa) than G5 dendrimers (MW 28 kDa), but with sufficient surface functional groups for attachment of additional functional

agents such as imaging, targeting, and therapeutic molecules. In order to validate the choice of dendrimer generation for *in vivo* biodistribution studies, we compared the penetration efficiency of G4 and G5 dendrimers in MCTS. We then conducted a biodistribution study in healthy mice to investigate the *in vivo* fate of the hybrid NPs encapsulating nontargeted G4 dendrimers compared to free dendrimer conjugates and empty NPs following a single intravenous (IV) injection up to 24 h. Finally, the *in vivo* targeting efficacy of the FA-targeted hybrid NPs was validated using athymic nude mice carrying xenografts of KB FR^+ tumors by comparing the targeted hybrid NPs, FA-targeted free dendrimers, and empty PEG-PLA NPs. This study presents the first *in vivo* results of the newly designed hybrid NPs.

2. EXPERIMENTAL METHODS

2.1. Materials

G4 and G5 PAMAM dendrimers, rhodamine B isothiocyanate (RITC), folic acid (FA), glycidol, tin(II)2-ethylhexanoate, poly(ethylene glycol) monomethyl ether (mPEG) (MW 5,000 Da), poly(vinyl alcohol) (PVA, 87–89% hydrolyzed, MW 13,000–23,000 Da), dimethyl sulfoxide (DMSO), dimethylformamide (DMF), and dichloromethane (DCM) were all obtained from Sigma-Aldrich (St. Louis, MO). *D,L*-lactide and Boc-NH-PEG5K-OH were purchased from Polysciences Inc. (Warrington, PA) and Jenkem Technology (Beijing, China), respectively. All other chemicals used in this study were purchased from Sigma-Aldrich unless specified otherwise.

2.2. Preparation of G4 and G5 PAMAM dendrimer conjugates

Fully hydroxylated RITC-labeled FA-targeted and nontargeted G4 and G5 PAMAM dendrimer conjugates (G4-RITC-FA-OH, G4-RITC-OH, G5-RITC-FA-OH, and G5-RITC-OH) were prepared and characterized as reported in our earlier publications. [27, 28] Conjugation of RITC and FA to the dendrimers and successful end-capping of the amine groups were confirmed using ^{1}H NMR (400 MHz Bruker DPX-400 spectrometer, Bruker BioSpin Corp., Billerica, MA), UV/Vis (DU800 UV/Vis Spectrophotometer, Beckman Coulter, CA), and zeta potential measurements (Table 1, Supporting Information Figure S1, Figure S2, and Figure S3). UV/Vis spectra revealed that the conjugates prepared in this study contained approximately 3.4 RITC and 5.8 FA molecules per G4 dendrimer, and 2.8 RITC and 5.9 FA molecules per G5 dendrimer (Supporting Information Figure S3).

2.3. Synthesis of PEG-PLA and RITC-PEG-PLA

PEG-PLA and Boc-NH-PEG-PLA were prepared by ring opening polymerization of *D,L*-lactide as previously described. [27, 28] RITC-PEG-PLA was then prepared following deprotection of Boc-NH-PEG-PLA as reported earlier. [28] ^{1}H NMR was used to confirm the chemical structure of the copolymers and to estimate the MW of the PLA block (Supporting Information Figure S4). This was calculated to be 44,900 g/mol for PEG-PLA and 48,800 g/mol for Boc-NH-PEG-PLA based on the relative integration ratios of peak b around 3.62 ppm (the protons of the ethylene oxide repeating units) to peak c around 5.15 ppm (the lactide repeating units). Following deprotection of Boc-NH-PEG-PLA, H_2N-PEG-

PLA was obtained and conjugated to RITC, which was also confirmed using ^{1}H NMR (Supporting Information Figure S4).

2.4. Encapsulation of the dendrimer conjugates into PEG-PLA NPs

Hybrid NPs containing targeted or nontargeted dendrimer conjugates (G4-RITC-FA-OH or G4-RITC-OH) were prepared using a double emulsion method as previously reported. [27–29] For example, G4-RITC-FA-OH (1 mL, 3 mg/mL in ddH_2O) was added to 5 mL of 10 mg/mL solution of PEG-PLA in DCM, and the mixture was sonicated for 1 min using a Misonix XL Ultrasonic Processor (100% duty cycle, 475 W, 1/8″ tip, QSonica, LLC, Newtown, CT). Ten milliliters of 3% aqueous PVA solution was then added to the mixture, followed by additional sonication for 1 min. The double emulsion was poured into 20 mL of 0.3% PVA in ddH_2O, and vigorously stirred at RT for 24 h to evaporate DCM. Unencapsulated dendrimers and PVA were removed by ultracentrfugation, with repeated washing with ddH_2O fifteen times. The resulting hybrid NP solution was redissolved in ddH_2O, lyophilized over 2 days, and stored at −20 °C. G4-RITC-OH was also encapsulated into PEG-PLA NPs using the same method. Empty RITC-NPs (50% w/w RITC-PEG-PLA) were prepared by adding ddH_2O instead of the dendrimer solution.

2.5. Structure confirmation and size/surface charge measurements

The dendrimer conjugates and PEG-PLA copolymers were characterized by ^{1}H NMR as previously described. [27–29] The structure of G4-RITC-FA-OH and G5-RITC-FA-OH was also confirmed by UV/Vis. The number of RITC and FA molecules attached to each dendrimer was calculated based on a standard curve of RITC and FA absorbance versus concentration in ddH_2O at 556 nm and 275 nm, respectively. Particle size (diameter, nm) and surface charge (zeta potential, mV) of the conjugates and the hybrid NPs were measured in triplicates by quasi-elastic laser light scattering using a Nicomp 380 Zeta Potential/ Particle Sizer (Particle Sizing Systems, Santa Barbara, CA) in ddH_2O. The measurements were performed using samples that were suspended in ddH_2O at a concentration of 100 μg/mL, filtered through a 0.45 μm syringe filter, and briefly vortexed prior to each measurement.

Loading efficiencies of G4 dendrimer-encapsulated hybrid NPs—Two milligrams of lyophilized hybrid NPs was dissolved in 1 mL of 0.5 M NaOH to degrade the PEG-PLA and completely release the loaded dendrimers, followed by filtration through a 0.45 μm syringe filter. The fluorescence intensity from the filtrates was then measured using a BioTek Synergy 4 microplate spectrofluorometer (Winooski, VT). The amount of the dendrimer conjugates in the filtrates was determined from a standard curve of each conjugate's fluorescence versus concentration in 0.5 M NaOH at 540 nm excitation and 590 nm emission wavelengths. Loading was expressed as mg dendrimer conjugates per mg copolymer. Loading efficiency was defined as the ratio of the actual loading obtained to the theoretical loading.

2.6. Cell culture

The KB cell line was purchased from the American Type Tissue Collection (ATCC, Manassas, VA) and grown continuously as a monolayer at 37 °C, 5% CO_2 in GIBCO FA-

deficient RPMI 1640 medium (Invitrogen Corporation, Carlsbad, CA) supplemented with penicillin (100 units/mL), streptomycin (100 mg/mL), and 10% heat-inactivated fetal bovine serum (FBS) (Invitrogen), resulting in FR-overexpressing KB (KB FR^+) cells.

2.7. Penetration assay using multicellular tumor spheroids (MCTS)

MCTS formation was performed using the liquid overlay method as previously reported. [28, 30] KB FR^+ cells from a confluent T-75 flask were detached using trypsin-EDTA and resuspended in FA-deficient RPMI 1640 at a concentration of 6×10^3 cells/mL. Five hundred microliters of the cell suspension were transferred to 8-well chamber slides (Millicell EZ Slide, Millipore, Billerica, MA) coated with 1% agarose in complete FA-deficient RPMI 1640. The cells were then incubated on agarose for 5 days to allow the formation of MCTS. After 5 days, 250 μL of the media in each well were removed, and MCTS were treated with 250 μL of 200 nM G4-RITC-FA-OH, G5-RITC-FA-OH, and the control conjugates G4-RITC-OH and G5-RITC-OH, for 1, 4, and 24 h. After each treatment, MCTS were carefully washed twice with PBS with Ca^{++}/Mg^{++}, fixed in paraformaldehyde for 10 min, and washed again. The chamber gasket was then removed, and the pieces of agarose were transferred to glass cover slips for confocal observation.

2.8. Confocal microscopy observations

Tumor spheroids were visualized using a Zeiss LSM 510 Meta confocal laser scanning microscope (CLSM, Carl Zeiss, Germany). The 543 nm line of a 1 mW tunable HeNe laser was used for the excitation of RITC, and emission was filtered at 565–595 nm. Images were captured using a 10x/0.25 Ph1 A-Plan objective, and Z-stack images were taken at 20 μm intervals for a total slice thickness of 200 μm.

2.9. Animals

Female BALB/c healthy and BALB/c athymic nude mice (6–8 weeks old) were obtained from Harlan Laboratories (Indianapolis, IN). Animals were treated in accordance with the National Institutes of Health Guide for the Care and Use of Laboratory Animals and the established Institutional Animal Care and Use protocol at the University of Illinois at Chicago. Animals were housed in a temperature and light-controlled environment (12 h light: 12 h darkness) and were provided food and water *ad libitum*.

2.10. Biodistribution of nontargeted dendrimers and hybrid NPs in healthy animals

Female BALB/c mice (n = 5) were anesthetized with an intraperitoneal (IP) injection of ketamine/xylazine (50 mg/kg and 5 mg/kg, respectively) prior to each injection. Each animal was injected with 3.7 mg/kg of the nontargeted dendrimer conjugates (G4-RITC-OH) (in ~200 μL normal saline) or an equivalent dose of the hybrid NPs or RITC-NPs (~80 mg/kg in ~200 μL normal saline) via the tail vein. At 1, 8, and 24 h post-injection, animals were given a high dose of ketamine/xylazine (100 mg/kg and 10 mg/kg, respectively) IP. Blood was collected from the dorsal vein into heparin-coated BD Vacutainer® tubes (Franklin Lakes, NJ). After blood collection, cervical dislocation was performed to ensure death, and organs were harvested (heart, lung, liver, kidneys, spleen, ovaries) for analyses.

2.11. Biodistribution of FA-targeted dendrimers and hybrid NPs in a KB FR$^+$ xenograft model

Six- to eight-week-old female BALB/c athymic nude mice (n = 3) were kept on a FA-deficient diet upon arrival and throughout the study. [24] KB FR$^+$ cells from confluent T-150 flasks were suspended in PBS at a concentration of 2.5×10^7 cells/mL, and ~200 μL of the cell suspension was injected subcutaneously using a 30g needle into the right flank of each mouse. The tumors were allowed to grow for 2 weeks until reaching ~1 cm^3 in size. Each animal was then anesthetized as descried above and injected with 3.7 mg/kg G4-RITC-FA-OH (in ~200 μL normal saline) or an equivalent dose of the hybrid NPs or RITC-NPs (~80 mg/kg in ~200 μL normal saline) via the tail vein. At 1 and 24 h post-injection, animals were given a high dose of ketamine/xylazine (100 mg/kg and 10 mg/kg, respectively) IP. Blood was collected from the dorsal vein into heparin-coated BD Vacutainer® tubes. After blood collection, cervical dislocation was performed to ensure death, and tumors and organs were harvested (heart, lung, liver, kidneys, spleen, ovaries) for analysis.

2.12. Blood and tissue analysis

For analysis of the blood collected from animals treated with the free dendrimer conjugates, blood collected from each animal was centrifuged at 13200 rpm (5 min, 4 °C) and the concentration of dendriemr conjugates was calculated from plasma by measuring the fluorescence of the supernatant at 540 nm excitation and 590 nm emission wavelengths based on a standard curve of dendrimer fluorescence versus concentration in plasma collected from saline-treated controls. For the analysis of the blood collected from animals treated with the hybrid NPs and NPs, 100 μL of whole blood was incubated with an equal volume of 1 N NaOH to ensure degradation of the hybrid NPs and NPs overnight in a shaking incubator (100 rpm, 37 °C). One hundred microliters of each sample were then taken to measure the fluorescence as above. The amount of dendrimer conjugates in the hybrid NPs and the amount of RITC-NP in the blood samples was calculated based on standard curves of dendrimer conjugates and RITC-NP in NaOH-treated whole blood.

For the analysis of tumor and tissue samples, approximately 100 mg of each tissue was massed into microcentrifuge tubes, to which 300 μL of ddH_2O was added. The samples were homogenized on ice using a manual tissue homogenizer. In order to ensure NP degradation, tissue homogenates from animals treated with the hybrid NPs and RITC-NPs were incubated with an equal volume of 1 N NaOH overnight in a shaking incubator (100 rpm, 37 °C). Tissue homogenates were centrifuged at 13200 rpm (30 min, 4°C). Supernatants were then collected and the fluorescence was measured at 540 nm excitation and 590 nm emission wavelengths using a fluorescence plate reader. The amount of dendrimer conjugates (free or encapsulated) and RITC-NPs in each sample was calculated based on standard curves of each material in supernatants of tissues and KB FR$^+$ tumors collected from saline controls, and expressed as % injected dose (% ID)/g tissue.

3. RESULTS AND DISCUSSION

3.1. Penetration efficiency of dendrimers with different generations

The penetration efficiency of G4-RITC-FA-OH was tested using multicellular tumor spheroids (MCTS), and compared to G5-RITC-FA-OH that has been extensively investigated *in vitro* and *in vivo* for targeted drug delivery to tumors. [21, 23, 24, 31] In this study, the penetration assay was performed using the MCTS for quantitative measurements, partially due to the technical difficulty in accurately measuring the penetration depth from the in vivo tissue samples. As shown in Figure 3, both generations of FA-targeted PAMAM dendrimers show similar penetration efficiency (G4 showing slightly higher penetration at the 4 h time point) and kinetics starting from 1 h, and gradually increasing afterwards. In sharp contrast, nontargeted conjugates (G4-RITC-OH and G5-RITC-OH) exhibited significantly lower penetration ability and much slower uptake kinetics compared to their targeted counterparts. After 24 h, all conjugates showed a similar degree of penetration efficiencies due to nonspecific uptake. The significance of these observations is that the FA-targeted dendrimer conjugates exhibited a significantly enhanced tumor penetration as compared to their non-targeted counterparts, regardless of their size difference (G4 vs. G5). Furthermore, FA-targeted G4 dendrimer conjugates possessed a similar tumor penetration ability to G5, supporting that their validity as a choice of targeted vectors incorporated within our hybrid NP system for subsequent *in vivo* biodistribution studies.

3.2. Altered biodistribution of dendrimer-encapsulated hybrid NPs

The G4 PAMAM dendrimer conjugates were encapsulated into PEG-PLA copolymers to produce the hybrid NPs using a double emulsion method as described earlier. [27, 28] The resulting hybrid NPs exhibited controlled particle sizes of apporximately 70 nm in diameter and high loading efficiencies (59 – 84%), as listed in Table 1. The change in zeta potential values for the dendrimer conjugates before encapsulation (2.7 – 4.2 mV) compared to the hybrid NPs (−12.5 – −16.6 mV) indicated successful encapsulation. Empty, RITC-labeled PEG-PLA NPs (RITC-NPs) were also prepared and characterized by measuring the particle size and zeta potential (Table 1). Previous biodistribution studies using PAMAM dendrimers have shown that following IV administration, kidneys are the major organs of elimination, which is often associated with short blood residence times (<10% ID remaining within 24 h).[24, 32, 33] On the other hand, PEGylated polymeric NPs are mostly eliminated by the RES (liver and spleen) and are longer circulating. [34–36] In order to see whether the hybrid NPs can improve the elimination kinetics of the dendrimer conjugates, we first investigated the biodistribution and elimination of nontargeted hybrid NPs compared to free dendrimer conjugates and empty NPs in healthy mice. As shown in Figure 4A, following a single IV injection, the nontargeted dendrimer conjugates (G4-RITC-OH) were quickly cleared from the blood (<10% ID remaining) after 24 h, and appeared mostly in the kidneys, with minimal amounts found in the liver or spleen. In contrast, an equivalent dose of dendrimers encapsulated within the hybrid NPs displayed a markedly different biodistribution profile (Figure 4B), which more closely resembled the *in vivo* fate of the empty NPs (Figure 4C). Unlike the free dendrimer conjugates, the hybrid NPs and RITC-NPs persisted longer in the blood, with 18–23% ID found after 24 h, and they were both mostly eliminated by the liver and spleen, with some accumulation in the heart and lung.

These observations support the hypothesis that the hybrid NP system can protect the encapsulated dendrimers from premature systemic elimination. This protection could be attributed to the combination of the larger particle size and controlled release of the dendrimer conjugates from the PEG-PLA matrix. The size of the hybrid NPs is larger than the renal threshold, switching the elimination pathway to organs of the RES such as the liver and spleen from the kidney. The outer PEG layer also imparts stealth properties to the system, similar to the PEGylated RITC-NPs and other nanocarriers reported in the literature. [34, 35, 37] These findings support the design rationale of the hybrid NPs, where prolonged circulation time of dendrimer conjugates can be successfully achieved through this multi-scale design.

3.3. Enhanced targeting efficacy and tumor accumulation of FA-targeted hybrid NPs

Next, we tested the biodistribution of FA-targeted hybrid NPs in mice carrying human KB FR^+ tumors, compared to FA-targeted dendrimers and RITC-NPs. As shown in Figure 5A, free FA-targeted dendrimers (G4-RITC-FA-OH) were cleared even more rapidly than nontargeted conjugates (Figure 4A), with less than 5% ID remaining after 24 h. The faster elimination of FA-targeted dendrimers was attributed to the significant liver uptake (~15% ID was found in the liver after 24 h) due to the presence of FA receptors in the liver and other RES organs such as the spleen. [24] Only ~5% ID could be found in the tumor tissue after 1 h, and ~3% ID after 24 h, highlighting the limitation of using FA-targeted dendrimers for tumor targeting. The data from Figure 4B demonstrate that dendrimer-encapsulated hybrid NPs are shielded from elimination and subsequently achieved longer circulation times compared to the free conjugates. This led us to hypothesize that in the presence of tumors, FA-targeted hybrid NPs will achieve higher concentrations in the tumor tissue through a combination of prolonged circulation time and passive targeting. As shown in Figure 5B, FA-targeted hybrid NPs not only persisted longer in the blood (14% ID remaining after 24 h), but also a higher % ID was found in the tumor tissue (12% compared to 3% for the free conjugates). A similar biodistribution pattern was observed for RITC-NPs, including in tumor tissue (Figure 5C). Note that the blood concentrations of FA-targeted hybrid NPs in tumor-bearing mice were slightly lower than RITC-NPs and the levels obtained with the nontargeted systems in healthy animals (Figure 4B). This is likely due to the faster elimination of FA-targeted conjugates upon their release from the hybrid NPs, in addition to their significant accumulation at the tumor site.

The enhanced targeting efficacy of the hybrid NPs is attributed to the sequential utilization of passive and active targeting. The protective PEG-PLA matrix shields the targeted dendrimer conjugates from premature elimination, while providing a stealth layer to prolong the circulation. The larger size of the hybrid NPs allows them to accumulate at the tumor site through the EPR effect, where by controlling their release, FA-targeted dendrimer conjugates are able to selectively target individual cancer cells. Similar levels of nontargeted polymeric NPs were also found in the tumor tissue. However, the high molecular flexibility and favorable tissue penetration properties of dendrimers are expected to enable the hybrid NPs to achieve more efficient tumor penetration and targeting compared to the rigid NPs. This is supported by our previous findings from simulated penetration assays in MCTS, where only the FA-targeted dendrimers were able to penetrate deeper into the spheroids,

while the empty NPs remained clustered at the periphery. [28] Additionally, one can argue that nontargeted hybrid NPs will be able to achieve similar tumor concentrations to FA-targeted ones. However, as observed in Figure 3, without the targeting ligand, the nontargeted dendrimer conjugates have significantly lower penetration efficiency compared to the targeted conjugates. This further supports our argument that the synergistic combination of active and passive targeting within the hybrid NP system is essential to enhance the targeting efficacy of the individual nanocarriers.

4. CONCLUSIONS

We report on the *in vivo* targeting efficacy of novel FA-targeted dendrimer-biodegradable polymer hybrid NPs. The multi-scale hybrid NP system was designed to overcome the limitations of existing nanocarriers such as the short circulation time (dendrimers) and poor penetration efficiency (polymeric NPs). By encapsulating FA-targeted dendrimers within long circulating PEG-PLA NPs, the larger size of the hybrid NPs and the controlled release of the dendrimer conjugates prevent the premature renal elimination of dendrimers. This allows for sufficient concentrations to accumulate at the tumor site, through a combination of passive and active targeting. Thus, the hybrid NPs exhibited enhanced tumor accumulation and retention compared to free FA-targeted dendrimers. Compared to polymeric NPs, it is expected that the favorable tissue diffusion and penetration properties of dendrimer conjugates will impart superior targeting efficacy and more efficient tumor distribution of drug molecules, which will be the subject of our future investigations.

Supplementary Material

Refer to Web version on PubMed Central for supplementary material.

Acknowledgments

This work was supported by the Hans W. Vahlteich Research Fund from the University of Illinois at Chicago (UIC) and the UIC Chancellor's Multidisciplinary Discovery Fund. The research was conducted in a facility constructed with support from the NIH (grant# C06RR15482). The authors thank Ms. Eri Iwasaki for her assistance in the animal studies.

References

1. Peer D, Karp JM, Hong S, Farokhzad OC, Margalit R, Langer R. Nanocarriers as an emerging platform for cancer therapy. Nature Nanotech. 2007; 2:751–760.
2. Torchilin VP. Recent advances with liposomes as pharmaceutical carriers. Nat Rev Drug Discov. 2005; 4:145–160. [PubMed: 15688077]
3. Kataoka K, Harada A, Nagasaki Y. Block copolymer micelles for drug delivery: design, characterization and biological significance. Adv Drug Deliver Rev. 2001; 47:113–131.
4. Maeda H. Tumor-selective delivery of macromolecular drugs via the EPR effect: Background and future prospects. Bioconj Chem. 2010; 21:797–802.
5. Pearson RM, Sunoqrot S, Hsu H-j, Bae JW, Hong S. Dendritic nanoparticles: the next generation of nanocarriers? Ther Deliv. 2012; 3:941–959. [PubMed: 22946429]
6. Jin SE, Bae JW, Hong S. Multiscale observation of biological interactions of nanocarriers: From nano to macro. Microsc Res Techniq. 2010; 73:813–823.
7. Jain RK, Stylianopoulos T. Delivering nanomedicine to solid tumors. Nat Rev Clin Oncol. 2010; 7:653–664. [PubMed: 20838415]

8. Popovic Z, Liu WH, Chauhan VP, Lee J, Wong C, Greytak AB, Insin N, Nocera DG, Fukumura D, Jain RK, Bawendi MG. A Nanoparticle size series for in vivo fluorescence imaging. Angew Chem. 2010; 122:8831–8834.
9. Yuan F, Leunig M, Huang SK, Berk DA, Papahadjopoulos D, Jain RK. Microvascular permeability and interstitial penetration of sterically stabilized (stealth) liposomes in a human tumor xenograft. Cancer Res. 1994; 54:3352–3356. [PubMed: 8012948]
10. Pearson RM, Hsu H-j, Bugno J, Hong S. Understanding nano-bio interactions to improve nanocarriers for drug delivery. MRS Bull. 2014; 3910.1557/mrs.2014.9
11. Huo S, Ma H, Huang K, Liu J, Wei T, Jin S, Zhang J, He S, Liang XJ. Superior penetration and retention behavior of 50 nm gold nanoparticles in tumors. Cancer Res. 2013; 73:319–330. [PubMed: 23074284]
12. Wong C, Stylianopoulos T, Cui J, Martin J, Chauhan VP, Jiang W, Popović Z, Jain RK, Bawendi MG, Fukumura D. Multistage nanoparticle delivery system for deep penetration into tumor tissue. P Natl Acad Sci USA. 2011; 108:2426–2431.
13. Waite CL, Roth CM. PAMAM-RGD conjugates enhance siRNA delivery through a multicellular spheroid model of malignant glioma. Bioconj Chem. 2009; 20:1908–1916.
14. Dhanikula RS, Argaw A, Bouchard JF, Hildgen P. Methotrexate loaded polyether-copolyester dendrimers for the treatment of gliomas: Enhanced efficacy and intratumoral transport capability. Mol Pharm. 2008; 5:105–116. [PubMed: 18171013]
15. Tang L, Fan TM, Borst LB, Cheng J. Synthesis and biological response of size-specific, monodisperse drug-silica nanoconjugates. ACS Nano. 2012; 6:3954–3966. [PubMed: 22494403]
16. Huang K, Ma H, Liu J, Huo S, Kumar A, Wei T, Zhang X, Jin S, Gan Y, Wang PC, He S, Zhang X, Liang XJ. Size-dependent localization and penetration of ultrasmall gold nanoparticles in cancer cells, multicellular spheroids, and tumors in vivo. ACS Nano. 2012; 6:4483–4493. [PubMed: 22540892]
17. Tang L, Gabrielson NP, Uckun FM, Fan TM, Cheng J. Size-dependent tumor penetration and in vivo efficacy of monodisperse drug–silica nanoconjugates. Mol Pharm. 2013; 10:883–892. [PubMed: 23301497]
18. Wu W, Driessen W, Jiang X. Oligo(ethylene glycol)-based thermosensitive dendrimers and their tumor accumulation and penetration. J Am Chem Soc. 2014; 136:3145–3155. [PubMed: 24506735]
19. Al-Jamal KT, Al-Jamal WT, Wang JTW, Rubio N, Buddle J, Gathercole D, Zloh M, Kostarelos K. Cationic poly-l-lysine dendrimer complexes doxorubicin and delays tumor growth in vitro and in vivo. ACS Nano. 2013; 7:1905–1917. [PubMed: 23527750]
20. Hong S, Leroueil PR, Majoros IJ, Orr BG, Baker JR Jr, Banaszak Holl MM. The binding avidity of a nanoparticle-based multivalent targeted drug delivery platform. Chem Biol. 2007; 14:107–115. [PubMed: 17254956]
21. Majoros IJ, Myc A, Thomas T, Mehta CB, Baker JR Jr. PAMAM dendrimer-based multifunctional conjugate for cancer therapy: Synthesis, characterization, and functionality. Biomacromolecules. 2006; 7:572–579. [PubMed: 16471932]
22. Myc A, Douce TB, Ahuja N, Kotlyar A, Kukowska-Latallo J, Thomas TP, Baker JR Jr. Preclinical antitumor efficacy evaluation of dendrimer-based methotrexate conjugates. Anti-Cancer Drug. 2008; 19:143–149.
23. Quintana A, Raczka E, Piehler L, Lee I, Myc A, Majoros I, Patri AK, Thomas T, Mule J, Baker JR Jr. Design and function of a dendrimer-based therapeutic nanodevice targeted to tumor cells through the folate receptor. Pharm Res. 2002; 19:1310–1316. [PubMed: 12403067]
24. Kukowska-Latallo JF, Candido KA, Cao Z, Nigavekar SS, Majoros IJ, Thomas TP, Balogh LP, Khan MK, Baker JR Jr. Nanoparticle targeting of anticancer drug improves therapeutic response in animal model of human epithelial cancer. Cancer Res. 2005; 65:5317–5324. [PubMed: 15958579]
25. Kaminskas LM, McLeod VM, Porter CJH, Boyd BJ. Association of chemotherapeutic drugs with dendrimer nanocarriers: an assessment of the merits of covalent conjugation compared to noncovalent encapsulation. Mol Pharm. 2012; 9:355–373. [PubMed: 22250750]

26. Singh P, Gupta U, Asthana A, Jain NK. Folate and folate-PEG-PAMAM dendrimers: Synthesis, characterization, and targeted anticancer drug delivery potential in tumor bearing mice. Bioconj Chem. 2008; 19:2239–2252.
27. Sunoqrot S, Bae JW, Pearson RM, Shyu K, Liu Y, Kim DH, Hong S. Temporal control over cellular targeting through hybridization of folate-targeted dendrimers and PEG-PLA nanoparticles. Biomacromolecules. 2012; 13:1223–1230. [PubMed: 22439905]
28. Sunoqrot S, Liu Y, Kim DH, Hong S. In vitro evaluation of dendrimer–polymer hybrid nanoparticles on their controlled cellular targeting kinetics. Mol Pharm. 2013; 10:2157–2166. [PubMed: 23234605]
29. Sunoqrot S, Bae JW, Jin SE, Pearson RM, Liu Y, Hong S. Kinetically controlled cellular interactions of polymer-polymer and polymer-liposome nanohybrid systems. Bioconj Chem. 2011; 22:466–474.
30. Friedrich J, Seidel C, Ebner R, Kunz-Schughart LA. Spheroid-based drug screen: considerations and practical approach. Nat Protocols. 2009; 4:309–324.
31. Majoros IJ, Thomas TP, Mehta CB, Baker JR Jr. Poly(amidoamine) dendrimer-based multifunctional engineered nanodevice for cancer therapy. J Med Chem. 2005; 48:5892–5899. [PubMed: 16161993]
32. Kobayashi H, Kawamoto S, Jo SK, Bryant HL, Brechbiel MW, Star RA. Macromolecular MRI contrast agents with small dendrimers: Pharmacokinetic differences between sizes and cores. Bioconj Chem. 2003; 14:388–394.
33. Nigavekar SS, Sung LY, Llanes M, El-Jawahri A, Lawrence TS, Becker CW, Balogh L, Khan MK. H-3 dendrimer nanoparticle organ/tumor distribution. Pharm Res. 2004; 21:476–483. [PubMed: 15070099]
34. Gref R, Minamitake Y, Peracchia MT, Trubetskoy V, Torchilin V, Langer R. Biodegradable long-circulating polymeric nanospheres. Science. 1994; 263:1600–1603. [PubMed: 8128245]
35. Li YP, Pei YY, Zhang XY, Gu ZH, Zhou ZH, Yuan WF, Zhou JJ, Zhu JH, Gao XJ. PEGylated PLGA nanoparticles as protein carriers: synthesis, preparation and biodistribution in rats. J Control Release. 2001; 71:203–211. [PubMed: 11274752]
36. Owens DE III, Peppas NA. Opsonization, biodistribution, and pharmacokinetics of polymeric nanoparticles. Int J Pharm. 2006; 307:93–102. [PubMed: 16303268]
37. Gabizon A, Horowitz AT, Goren D, Tzemach D, Shmeeda H, Zalipsky S. In vivo fate of folate-targeted polyethylene-glycol liposomes in tumor-bearing mice. Clin Cancer Res. 2003; 9:6551–6559. [PubMed: 14695160]

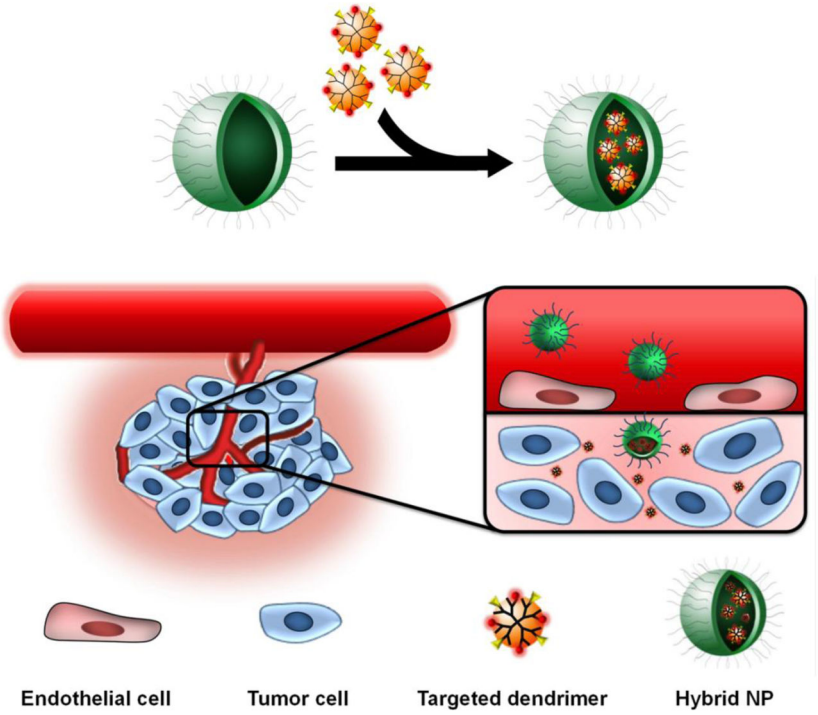

Figure 1.

A schematic illustration of the hybrid NP and sequential passive and active targeting enabled by the hybrid design. The PEGylated, larger NP shell allows the hybrid NPs to circulate long in the bloodstream and passively accumulate at the tumor site through the EPR effect. The actively targeted dendrimers can be released in a controlled manner, achieving active targeting to individual tumor cells and deep penetration within the tumor tissue, ultimately resulting in enhanced targeting efficacy.

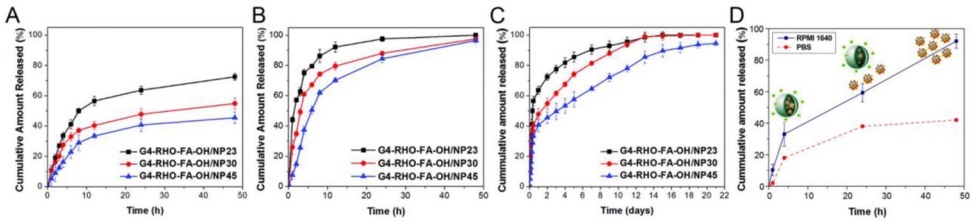

Figure 2.

Hybrid NPs display highly tunable controlled release kinetics. Release of folate targeted G4 PAMAM dendrimers encapsulated in hybrid NPs conducted in PBS buffer (A) or RPMI 1640 medium supplemented with 10% FBS (B) for 48 h, and in PBS buffer (C) for 21 days. Controlled release of folate targeted G4 PAMAM dendrimers from fluorescently labelled hybrid NPs following 48 h of incubation in RPMI 1640 or PBS buffer (D). Reprinted with permission from *Biomacromolecules*, 2012, **13,** 1223–1230 and *Molecular Pharmaceutics*, 2013, **10,** 2157–2166. Copyright (2012) and (2013) American Chemical Society.

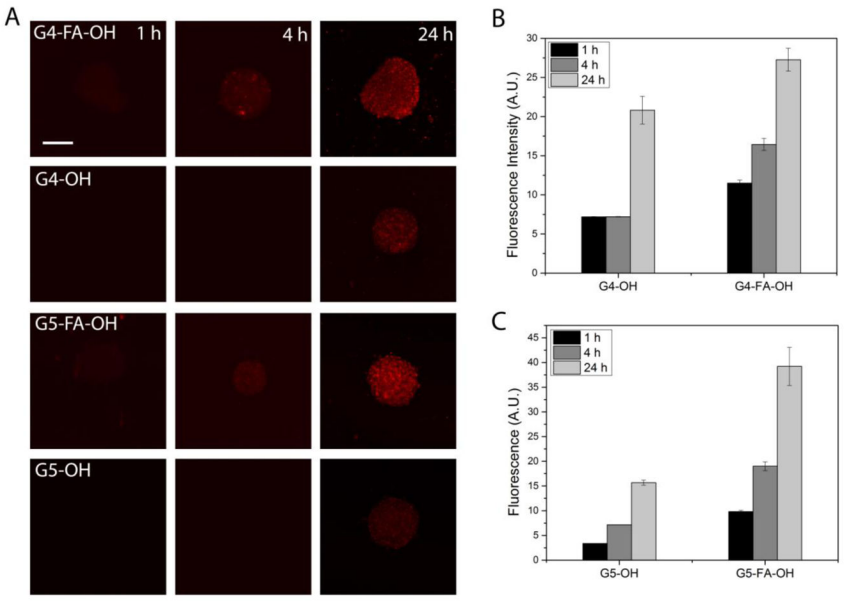

Figure 3.

(A) CLSM images of KB FR$^+$ MCTS upon incubation with G4-RITC-FA-OH (1st row), G4-RITC-OH (2nd row), G5-RITC-FA-OH (3rd row), and G5-RITC-OH (4th row) up to 24 h. Red: RITC-labeled dendrimers. Images shown were taken at a z-depth of 80 μm into each spheroid, scale bar: 100 μm. (B) Corresponding fluorescence count obtained by ImageJ. Both targeted dendrimer conjugates display significantly enhanced tumor penetration, compared to their nontargeted counterparts. Additionally, the G4-RITC-FA-OH conjugates displayed a penetration ability that was slightly better at 4 h and similar at 24 h, compared to the G5-RITC-FA-OH, validating their use as FA-targeted vectors in the hybrid NP system.

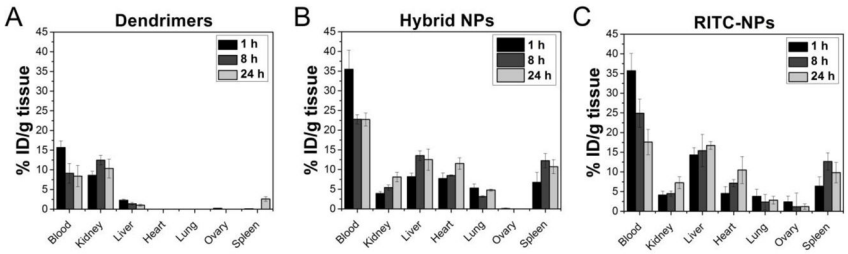

Figure 4.

Biodistribution profiles of (A) nontargeted G4 dendrimers (G4-RITC-OH), (B) nontargeted hybrid NPs, and (C) empty RITC-NPs, following a single IV injection. The nontargeted dendrimer conjugates were quickly cleared from the blood (<10% ID remaining) after 24 h, and found mostly in the kidneys. In contrast, an equivalent dose of dendrimers encapsulated within the hybrid NPs displayed a biodistribution profile closer to RITC-NPs. The hybrid NPs and RITC-NPs persisted longer in the blood, with 18–23% ID found after 24 h, and they are both mostly eliminated by the liver and spleen.

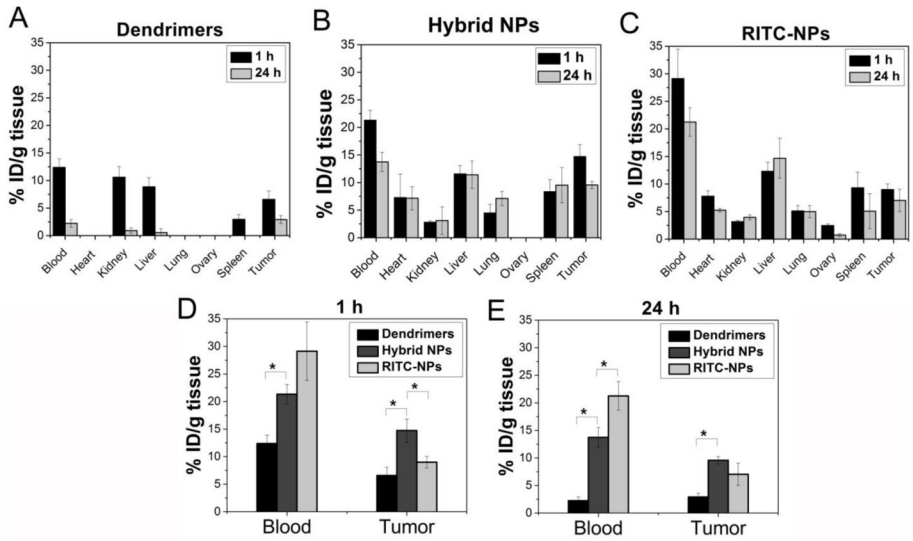

Figure 5.

Biodistribution profile of (A) FA-targeted G4 dendrimers (G4-RITC-FA-OH), (B) FA-targeted hybrid NPs, and (C) empty RITC-NPs, in BALB/c mice carrying human KB FR^+ xenografts, following a single IV injection. Delineated blood and tumor levels of the three groups after (D) 1 h and (E) 24 h of injection, $*p < 0.05$ based on a 1-way ANOVA followed by Tukey's post-hoc test. FA-targeted dendrimers (A) were cleared from the blood faster than nontargeted conjugates (Figure 3A), with < 5% ID remaining after 24 h, due to significant liver uptake (~15% ID). Only ~5% ID could be found in the tumor tissue after 1 h, and ~3% ID after 24 h. FA-targeted hybrid NPs (B) not only persisted longer in the blood (14% ID remaining after 24 h), but also a higher % ID was found in the tumor tissue (12%) compared to the free conjugates. A similar biodistribution pattern was observed for RITC-NPs, including in tumor tissue (C).

Table 1

Characterization of G4 and G5 PAMAM dendrimers and hybrid NPs

	Particle size (nm)	Zeta potential (mV)	Loading efficiency (%)
G4-RITC-OH	12.1 ± 7.3	4.2 ± 1.7	N/A
G4-RITC-FA-OH	16.3 ± 7.8	2.7 ± 1.5	N/A
G5-RITC-OH	13.1 ± 2.8	8.3 ± 4.6	N/A
G5-RITC-FA-OH	14.0 ± 2.9	2.8 ± 1.2	N/A
G4-RITC-OH/NP	71.6 ± 14.2	−16.6 ± 0.8	59.2
G4-RITC-FA-OH/NP	60.8 ± 10.3	−12.5 ± 2.4	83.8
RITC-NP	62.4 ± 14.1	−16.5 ± 1.5	N/A